DIAGNOSTYKA, 2016, Vol. 17, No. 3

ISSN 1641-6414
e-ISSN 2449-5220

DETECTION OF DEBONDING IN STEEL BARS EMBEDDED IN CONCRETE USING GUIDED WAVE PROPAGATION

Beata ZIMA, Magdalena RUCKA
Gdańsk University of Technology, Faculty of Civil and Environmental Engineering,
Department of Mechanics of Materials, Narutowicza 11/12, 80-233 Gdańsk, Poland,
e-mail: beazima@pg.gda.pl, mrucka@pg.gda.pl

Summary

The paper presents a non-destructive diagnostic technique based on guided wave propagation phenomenon used to assess the adhesive bonding between a steel bar and a concrete cover. Double-layered cylindrical specimens with different levels of debonding and its location were investigated. The influence of bonding length on the excitation of multiple modes of longitudinal guided waves was analysed. Numerical simulations of guided wave propagation in healthy and damaged specimens were conducted and differences in the occurring phenomena were specified. The analysis of the obtained results confirms the possibility to apply the guided wave propagation method in the assessment of degradation level in the adhesive bonding of multi-layered cylindrical structures.

Keywords: guided waves, non-destructive diagnostics, bar embedded in concrete, debonding

DETEKCJA ROZWARSTWIENIA W PRĘTACH STALOWYCH OSADZONYCH W BETONIE Z ZASTOSOWANIEM PROPAGACJI FAL PROWADZONYCH

Streszczenie

W artykule przedstawiono nieinwazyjną technikę diagnostyczną wykorzystującą zjawisko propagacji fal prowadzonych w ocenie stanu połączenia adhezyjnego pomiędzy stalowym zbrojeniem a otuliną betonową. Przeanalizowano dwuwarstwowe próbki cylindryczne z różnymi wielkościami i położeniami delaminacji między warstwami. Opisano także wpływ długości zakotwienia na wzbudzenie kolejnych modów podłużnych fal prowadzonych. Symulacje numeryczne propagacji fal zostały przeprowadzone dla prętów stalowych osadzonych w betonie w stanie bez uszkodzenia oraz z uszkodzeniem w postaci braku przyczepności między stalą a betonem. Wskazano na różnice w zachodzących zjawiskach propagacji fali w zależności od stopnia rozwarstwienia. Analiza uzyskanych rezultatów potwierdza możliwość wykorzystania zjawiska propagacji fal w ocenie stopnia degradacji połączeń adhezyjnych wielowarstwowych konstrukcji cylindrycznych.

Słowa kluczowe: fale prowadzone, diagnostyka nieniszcząca, pręt osadzony w betonie, rozwarstwienie

1. INTRODUCTION

The guided wave propagation method has been repeatedly and effectively applied for damage detection in the elements of civil and mechanical structures. The idea is based on the wave excitation in an object and the registration of vibrations at selected points of an investigated area. The appropriate interpretation of recorded reflections in signals brings about the information about possible defects, the presence of inclusions or areas with different material parameters. Due to relatively small reduction of the amplitude during propagation, and thus the possibility of monitoring a large area during a single measurement the guided waves are particularly useful for non-destructive inspection of metal objects. The estimation of the corrosion level in reinforcing steel bars is presented by Umar et al. [1]. Liu et al. [2] described a detection method for plate structures with rectangular phased array transducers. Hall and Michaels [3] introduced a multipath guided wave imaging to detect damage in aluminium plates. Zima and Rucka [4] applied wavelet signal processing of guided waves for notch detection in steel plates. Kędra and Rucka [5] presented the results of guided wave inspection of a bolted lap joint. All above mentioned cases refer to testing of metal structures. However, most real structural elements are made of two or more materials of different characteristics. A need emerges to develop diagnostic techniques dedicated to the assessment of the state of such facilities. Attempts of the use of guided wave propagation to assess the condition of composite structures include inspection of embedded profiles [6], reinforced concrete beams [7], rock bolts and ground anchors [8-13].

A significant and common problem of coated waveguides is debonding between distinct layers. The paper concerns the assessment of adhesive bonding between steel bars and a concrete cover by means of guided wave propagation method. Double-layered cylindrical specimens with variable level of debonding and its location are investigated

numerically using the Finite Element Method. The aim of the study is to investigate the influence of bonding length on the excitation of multiple modes of longitudinal guided waves.

2. DISPERSION RELATIONS FOR CYLINDRICAL WAVEGUIDES

Guided waves exhibit dispersive character and their propagation velocity depends on the frequency. Moreover, in the predominant frequency range, in the waveguide more than one mode can propagate. In order to determine the number of propagating modes and their velocities, dispersive equations must be solved and dispersive curves must be analysed.

The dispersion relation for isotropic rods of solid, circular cross-sections has been derived independently by Pochhammer [14] and Chree [15]. The relation for a cylindrical rod with a radius r, modulus of elasticity E, mass density ρ and Poisson's ratio ν takes the following form:

$$\begin{aligned}&\frac{2\alpha}{r}\left(\beta^2+k^2\right)J_1(\alpha r)J_1(\beta r)+\\&-\left(\beta^2-k^2\right)^2 J_0(\alpha r)J_1(\beta r)+\\&-4k^2\alpha\beta J_1(\alpha r)J_0(\beta r)=0,\end{aligned} \tag{1}$$

where J_0 and J_1 are Bessel's functions of the first kind and parameters α and β are:

$$\alpha^2=\frac{\omega^2}{c_L^2}-k^2,\quad \beta^2=\frac{\omega^2}{c_S^2}-k^2 \tag{2}$$

The wavenumber k relates the circular frequency ω to its phase velocity c:

$$k=\frac{\omega}{c}, \tag{3}$$

and the group velocity c_g can be calculated as:

$$c_g=\frac{d\omega}{dk}. \tag{4}$$

Velocities of the pressure and shear waves are given by relations:

$$c_L=\sqrt{\frac{E(1-\nu)}{\rho(1+\nu)(1-2\nu)}}, \tag{5}$$

$$c_S=\sqrt{\frac{E}{2\rho(1+\nu)}}. \tag{6}$$

The solution of Eq. (1) may be presented graphically in the form of the so-called dispersion curves relating the phase or group velocity of a propagating wave vs. the wave frequency. Figure 1 presents dispersion curves for a circular cross-section steel rod with a diameter of 2 cm. In the presented frequency range up to 200 kHz, two longitudinal modes are visible. Group velocity of the first mode $L(0,1)$ decreases with the increase of frequency. The second mode $L(0,2)$ appears above the cut-off frequency equal to 180 kHz.

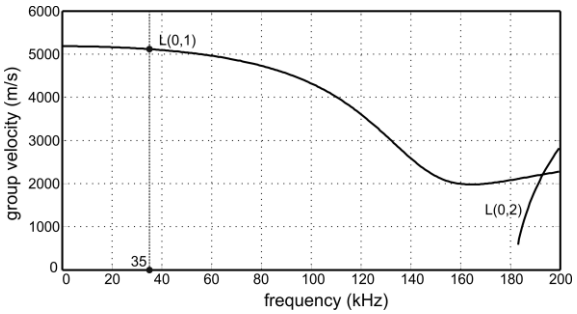

Fig. 1. Dispersion curves for a steel 2 cm diameter rod (E = 210 GPa, ν = 0.3, ρ = 7820 kg/m^3)

Dispersion equations for multi-layered cylindrical waveguides are much more complex than the Pochhammer equation and their solution causes many difficulties (e.g. [16, 17]). In the study the dispersion curves for a steel rod embedded in concrete casting were plotted using free software PCdisp [18]. Figure 2 shows that the presence of additional layer in the form of concrete cover causes a significant increase in the number of propagating modes and thus increase in the complexity of the occurring phenomena. The cut-off frequencies for higher modes correspond to lower values than in the case of a free rod, therefore in the considered frequency range from 0 kHz to 200 kHz 13 modes can propagate. Moreover, the velocity of the fastest $L(0,1)$ mode is significantly lower than the velocity of $L(0,1)$ mode in the rod without a cover.

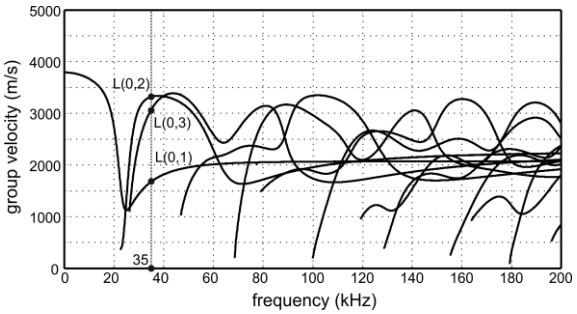

Fig. 2. Dispersion curves for a steel 2 cm diameter rod (E = 210 GPa, ν = 0.2, ρ = 7820 kg/m^3) embedded in concrete cover with 4 cm thickness (E = 26 GPa, ν = 0.2, ρ = 2084 kg/m^3)

3. WAVE PROPAGATION IN WAVEGUIDES WITH DIFFERENT BONDING LENGHTS

When a wave propagates in a rod embedded in a cover of different material parameters, part of the energy is transmitted into surrounding medium in the form of outgoing waves. The longer the cover, the more intensive wave leakage is observed. The energy leakage into the adjacent medium depends not only on the length of the connection but also on its quality. High quality of the connection facilitates the transfer of energy. Thus the amplitude value of the registered signal may be considered as indirect parameter indicating the bonding length.

This section presents schematic diagrams illustrating propagation of wave packets in a two-layered perfectly bonded specimen and specimens with emerging debonding. In the case of the specimen with perfect bonding between the waveguide and the cover after excitation of a wave at one end of the rod, certain modes start propagating (Fig. 3). The number of propagating modes depends on the excitation frequency and is a result of the dispersive nature of guided waves. The example presented in Fig. 3 concerns the case of the excitation frequency equals to 35 kHz, according to situation indicated in Fig. 2. For this frequency three modes propagate with different group velocities c_{g_i}. The highest group velocity has mode $L(0,2)$ and the lowest velocity – mode $L(0,1)$. As the wave travels through the specimen of a length L, the registration time of individual wave packets is equal to:

$$t_i = \frac{L}{c_{g_i}}. \tag{7}$$

The time interval between registration times of particular modes i and j can be calculated as:

$$\Delta t_{i-j} = \left| \frac{L(c_{g_j} - c_{g_i})}{c_{g_i} c_{g_j}} \right|. \tag{8}$$

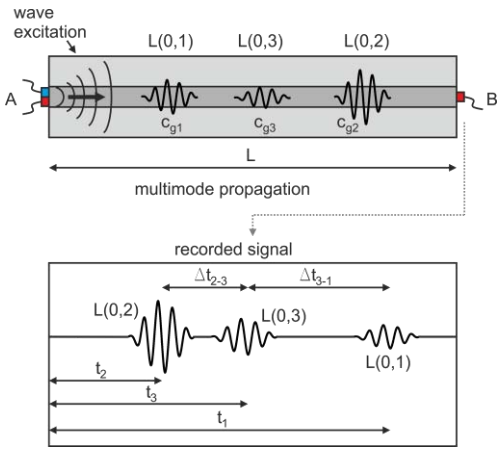

Fig. 3. Wave propagation in the rod perfectly bonded with concrete cover

When the bonding connection is damaged on a certain length, other phenomena associated with wave propagation occur. Moreover, the position of debonding will act strongly on the results. The first damage scenario (Fig. 4) concerns debonding occurring at the end of the specimen, at which the actuator is attached. For a given frequency the number of propagation modes in the free rod is always smaller than the number of modes propagating in the rod embedded in a coating material (cf. Fig. 1 and Fig. 2). Therefore only one mode initially propagates along the free length L_f of the rod with the group velocity equal to c_{g_f} (Fig. 4a). When the wave packet reaches the place where the rod is anchored in the cover, it diffracts in accordance to Huygens principle (Fig. 4b). Part of its energy propagates forward and back in the cover while the remaining part propagates along the embedded rod. The energy of the diffracted wave is separated into several modes, which propagate with different group velocities c_{g_1}, c_{g_2}, c_{g_3}. The signal registered at point B for damaged specimen is presented in Fig. 4c. As the wave travels through the specimen of a length L, the registration time of individual wave packets is:

$$t_{d_i} = \left| \frac{Lc_{g_f} - L_f(c_{g_f} - c_{g_i})}{c_{g_f} c_{g_i}} \right|. \tag{9}$$

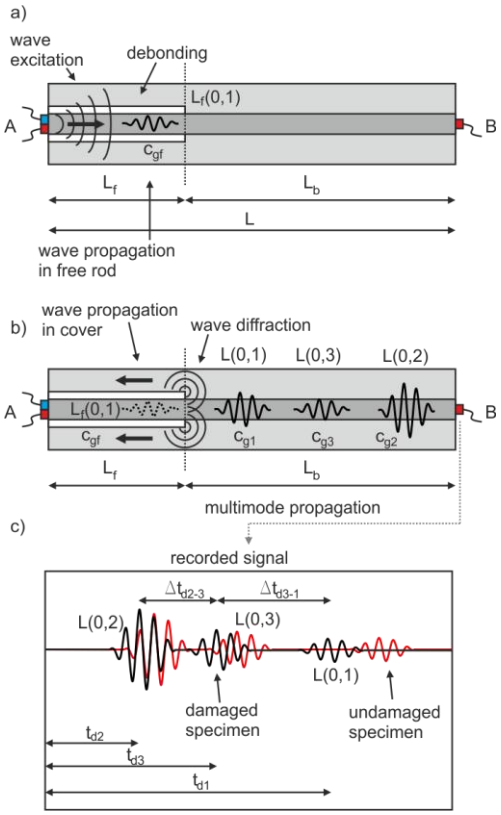

Fig. 4. Wave propagation in the rod embedded in concrete cover with debonding at one end of the rod

As long as the propagation velocity in the free rod c_{g_f} is higher than the propagation velocity in coated rod c_{g_i}, the registration time t_{d_i} is shorter for longer delaminated section. For damaged specimen individual wave packets are registered earlier than for undamaged specimen (Fig. 4c).

The difference in registration times between individual modes *i* and *j* for the damaged specimen is:

$$\Delta t_{d_{i-j}} = \left| \frac{L_b (c_{g_j} - c_{g_i})}{c_{g_i} c_{g_j}} \right|. \tag{10}$$

Eq. (10) says that the longer bonding length L_b, the higher time interval between particular modes, so they propagate as separate wave packets. In the case of substantial debonding (Fig. 5a), the time intervals are short, so particular modes may be registered as a single wave packet (Fig. 5b). The same effect would be observed for small difference between group velocities of excited modes.

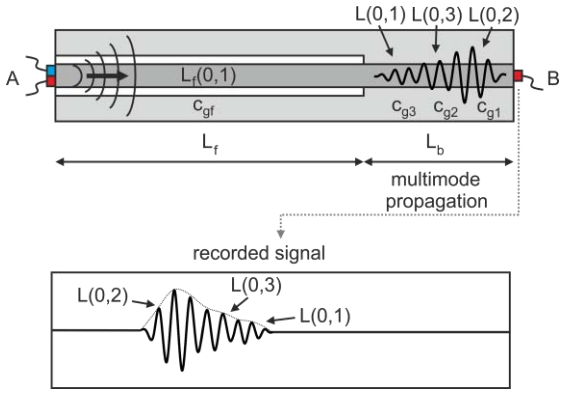

Fig. 5. Wave propagation in the rod embedded in concrete cover with debonding of considerable length at one end of the rod

The second damage scenario (Fig. 6) refers to the case of the debonding occurring in the middle part of the element. After wave excitation, several modes propagate with different group velocities along the bonding length L_{b_1} (Fig. 6a). When the wave reaches the place where the rod is not connected with the cover, only the free rod modes propagate, while higher order modes disappear (Fig. 6b). Next, several modes propagate along the bonding length L_{b_2} again (Fig. 6c). When debonding occurs in the middle part of the specimen, wave diffracts at two ends of the defect. The diffracted wave can be registered as an additional wave packet. Moreover, after diffraction, another part of the energy propagates in the cover and the part of energy propagates in the rod (Fig. 6b). The propagation velocity of these waves differs, due to material parameters of the cladding and the core. When the waves reach the end of the delaminated part, it diffracts again (Fig. 6c). The relations govering registration times of wave packets and differences between registration times are identical to the first damage scenario (Eqs. 9 and 10). The complexity of the obtained results is much larger in this case because of multimode propagation, multiple reflections and wave diffraction.

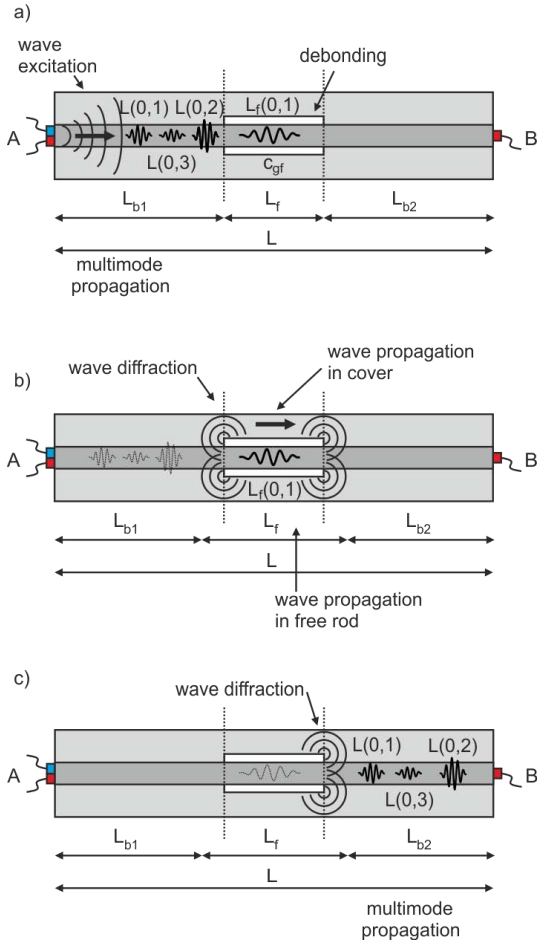

Fig. 6. Wave propagation in the rod embedded in concrete cover with debonding at the middle part

4. FEM MODEL

Numerical calculations were performed by means of Finite Element Method in Abaqus/Explicit programme. Four-node axisymmetric finite elements with reduced integration (CAX4R) were applied here. Analysis was conducted for a 2 cm diameter steel rod (E = 210 GPa, ν = 0.2, ρ = 7820 kg/m^3) embedded in concrete cover (E = 26 GPa, ν = 0.2, ρ = 2084 kg/m^3) with a thickness equal to 4 cm. The length of the specimen was equal to 1 m. Four different models were investigated: free rod (model #1), rod perfectly bonded with the cover (model #2), two-layered rod with debonding at one end of the specimen (model #3) and two-layered rod with debonding in the middle part of the specimen (model #4). Additionally, in the case of models with debonding (models #3 and #4), four different levels of state deterioration were considered (delaminated part of the rod L_f was equal to 20, 40, 60 and 80 cm). The wave was excited and registered at the steel rod, in the longitudinal direction. The wave

packet consisted of five-cycle sine with a carrier frequency equal to 35 kHz modulated by the Hanning window.

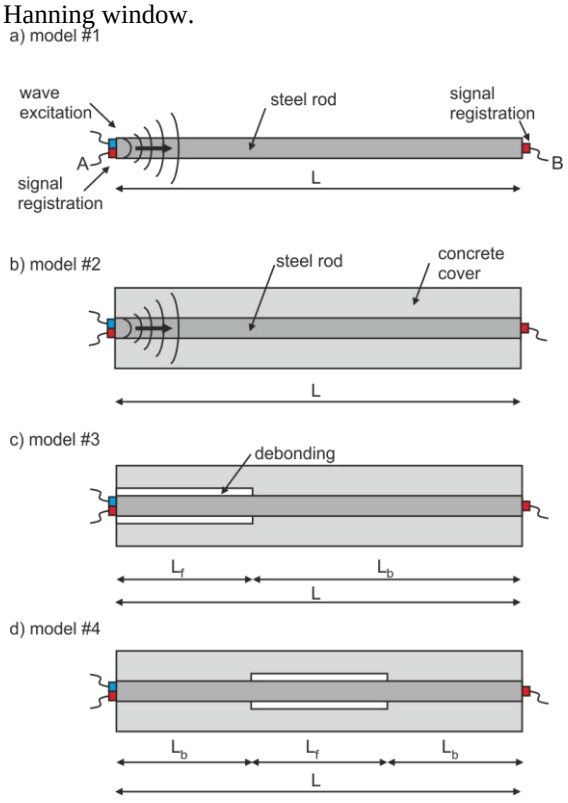

Fig. 7. Analysed specimens: a) free rod; b) rod perfectly bonded with concrete cover; c) rod embedded in concrete cover with debonding at one end of the rod; d) rod embedded in concrete cover with debonding at the middle part of the rod

5. RESULTS AND DISCUSSION

Results of FEM simulations are presented in the form of acceleration maps at selected time instances as well as in the form of signals measured at the end of the rod. Because of the considerable amplitude decay resulting from the energy leakage during wave propagation, in acceleration maps for each snapshot different scale factor was introduced to provide better visibility. Moreover, deformations caused by wave motion were introduced in maps in order to enhance the observation and recognition of particular modes.

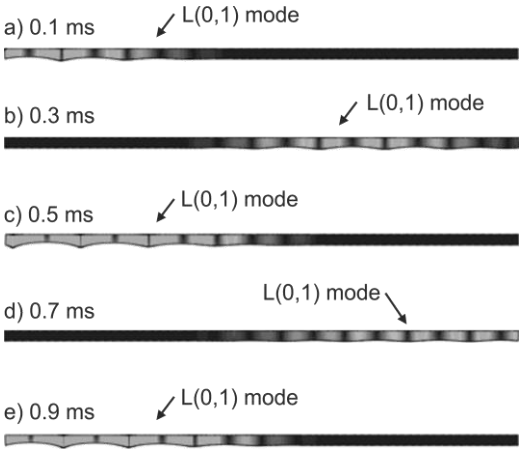

Fig. 8. Wave propagation in the free rod (model #1)

Results for the free rod are presented in Fig. 8. For 35 kHz excitation frequency only one mode L(0,1) propagates in the waveguide with the group velocity of 5104.6 m/s. Wave propagation patterns for the rod perfectly bonded with the cover are shown in Fig. 9. Excitation of the wave packet of a frequency of 35 kHz results in propagation of three modes of the longitudinal wave. At the beginning (t = 0.1 ms) a single wave packet containing all three modes is visible only (Fig. 9a). After 0.2 ms two modes $L(0,2)$ and $L(0,3)$ can be distinguished (Fig. 9b). Three separate wave modes are visible after 0.72 ms (Fig. 9e).

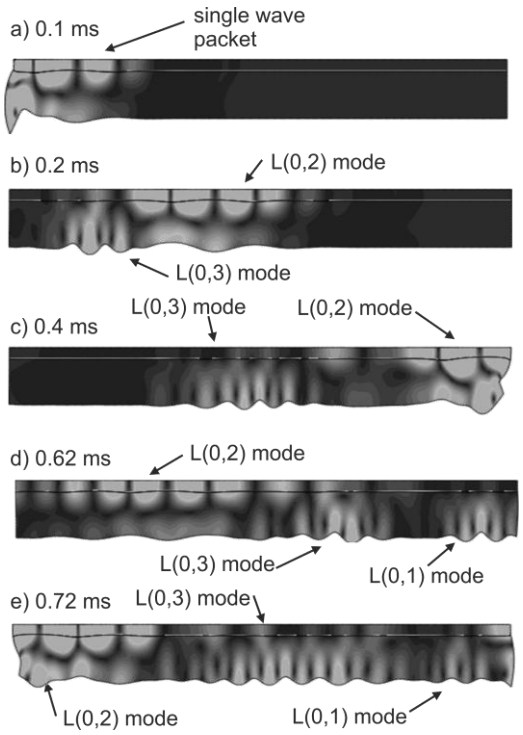

Fig. 9. Wave propagation in the rod perfectly bonded with concrete cover (model #2)

The wave propagation signal registered at the end of the rod by sensor B is presented in Fig. 10. All the three modes were identified. However, due to small difference in group velocities of $L(0,2)$ and $L(0,3)$ modes, the interference occurs, so combined wave packets are visible. Moreover, a relatively small value of the amplitude of $L(0,3)$ mode makes it difficult to identify in the signal.

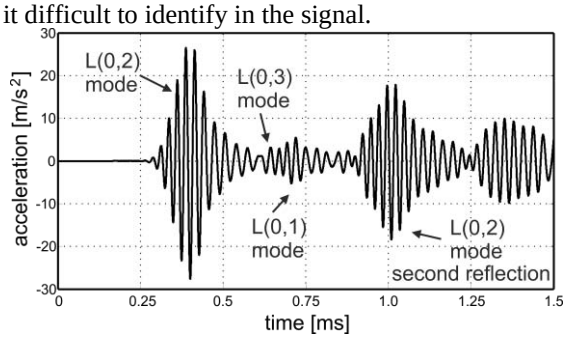

Fig. 10. Signal registered by sensor B in the rod perfectly bonded with concrete cover (model #2)

Snapshots of propagating waves in the rod embedded in concrete cover with debonding at one end of the rod are shown in Figs. 11 and 12, for two different lengths of defects (L_f = 80 and 40 cm).

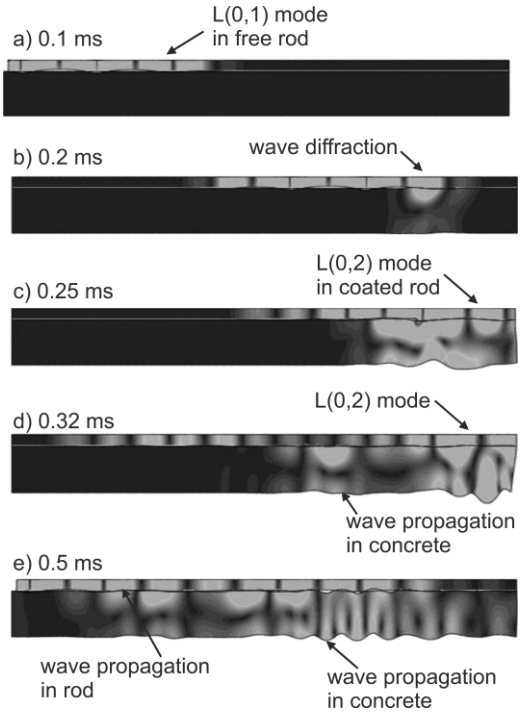

Fig. 11. Wave propagation in the rod embedded in concrete cover with debonding at one end of the rod (model #3, L_f = 80 cm)

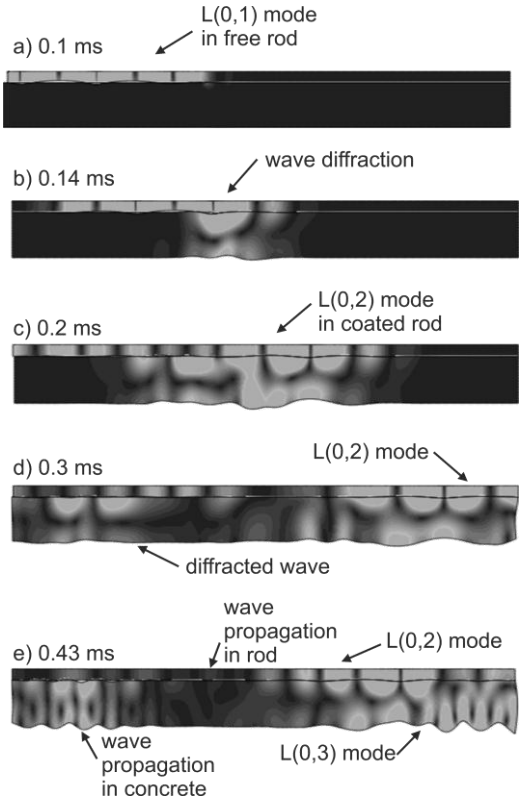

Fig. 12. Wave propagation in rod embedded in concrete cover with debonding at the one end of the rod (model #3, L_f = 40 cm)

At the beginning (t = 0.1 ms) only $L(0,1)$ mode in the free rod propagates (Figs. 11a and 12a). While it reaches the end of debonding, the wave diffraction is visible (Figs. 11b and 12b). After diffraction part of the energy propagates back in the concrete cover while remaining the part propagates in the two-layer rod. In the first phase of propagation in bonded length, only $L(0,2)$ mode with the highest velocity is distinguishable. For the rod with shorter bonding length (L_b = 20 cm) separate modes are impossible to identify (Fig. 11), but in the second specimen the bonding length (L_b = 60 cm) was long enough to enable a separation both $L(0,2)$ and $L(0,3)$ modes (Fig. 12).

Wave propagation signals registered at the embedded end of the specimens with different levels of debonding are presented in Fig. 13. The fastest $L(0,2)$ mode is also characterized by a higher amplitude value. The modes $L(0,1)$ and $L(0,3)$ have amplitudes comparable to the amplitude of a damage-diffracted wave. A significant amplitude peak is also registered after the second reflection of $L(0,2)$ mode from the end of the rod. The amplitude of the first wave packet of $L(0,2)$ mode decreases with the increase of the bonding length as a result of a more intensive wave leakage into surrounding medium. However, for the rod with perfectly bonded layers, the amplitude of this wave packet is comparable with the amplitude registered for the rod with the shortest bonding length. This came from the fact that significant amount of the energy is

dissipated due to wave leakage but also because of the wave diffraction corresponding to debonding.

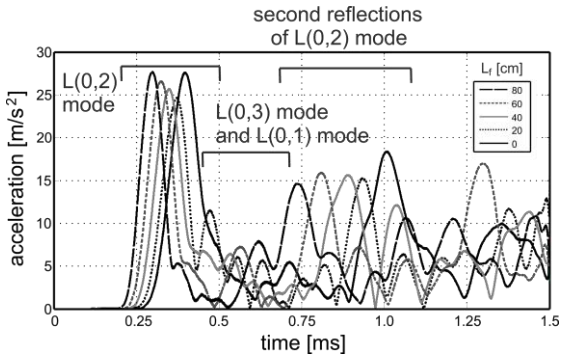

Fig. 13. Envelopes of signals registered by sensor B in specimen #3 with different levels of debonding

Figures 14 and 15 illustrate guided waves propagated in the rod embedded in concrete with debonding at the middle part, for two different lengths of defects (L_f = 80 and 40 cm respectively). After excitation, a single wave packet containing all three modes propagates in the first bonding length of the specimen. After the first diffraction, part of the energy propagates in concrete while the other part propagates as $L(0,1)$ mode in the free part of the rod (Figs. 14b and 15b). When the wave reaches the location of perfect connection between steel and concrete, the second diffraction takes place and again the single wave packet propagates in specimen (Fig. 14c and 15c). When the bonding length is long enough, the separation of particular modes can be observed, as presented in Fig. 15e.

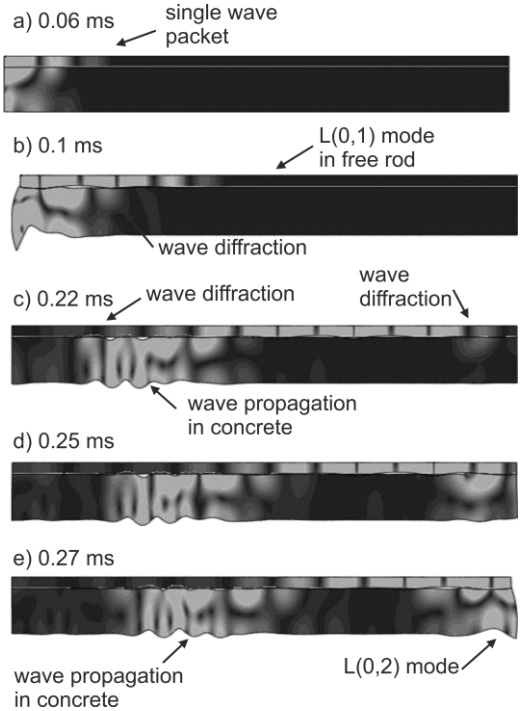

Fig. 14. Wave propagation in rod embedded in concrete cover with debonding at the middle part (model #4, L_f = 80 cm)

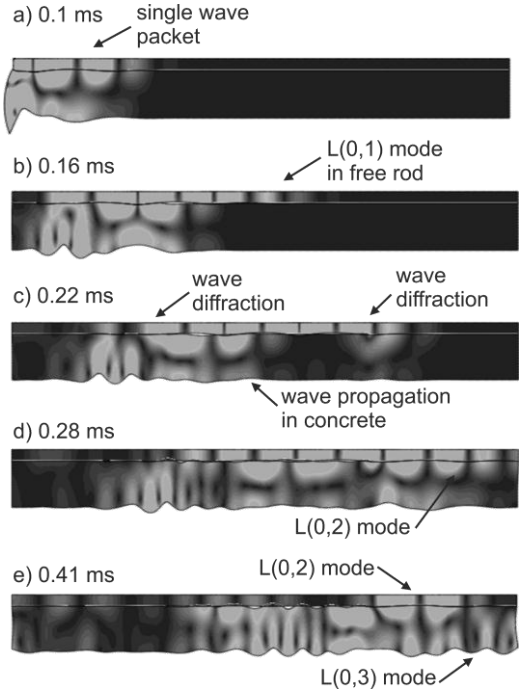

Fig. 15. Wave propagation in rod embedded in concrete cover with debonding at the middle part (model #4, L_f = 40 cm)

Envelopes of signals registered at the end of the rod with different levels of debonding are given in Fig. 16. Only $L(0,2)$ mode and its second reflection are easy to identify while indication of $L(0,3)$ and $L(0,1)$ modes is much more complicated because of multiple diffractions and additional disturbance propagation in the concrete part.

Although the debonding length was identical for models #3 and #4, there are significant differences in the wave propagation process occurrence. When the debonding develops at the end of the rod, signals are relatively easy to interpret in comparison with signals registered for the specimen debonded at the middle part. Moreover, it is clearly visible that amplitude values of $L(0,2)$ mode are lower in the case of the middle positioned debonding (cf. Fig. 13 and Fig. 16). Damage occurring in the middle part of the element produced higher energy dissipation due to the multiple wave diffraction.

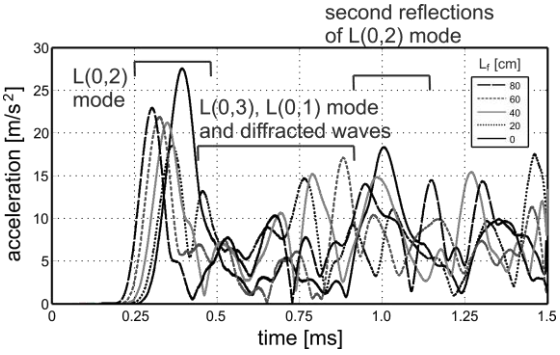

Fig. 16. Envelopes of signals registered by sensor B in specimen #4 with different levels of debonding

6. CONCLUSIONS

The paper presents theoretical and numerical investigation in the field of guided wave propagation in double-layered cylindrical structures. The steel bar embedded in the concrete cover has been analysed due to different scenarios of debonding between core and cladding. Numerical studies have shown that in damaged specimens different types of modes propagate in free and bonded sections of the rod. The influence of size and position of the debonding on the excitation of multiple modes of longitudinal guided waves has been investigated. The study revealed that the parameter identifying the quality of multi-layered specimens in the amplitude value, but also the level of signal complication and the time interval between propagating modes.

BIBLIOGRAPHY

1. Umar A., Yadav S.K., Kundu T. Detection and quantification of diameter reduction due to corrosion in reinforcing steel bars. *Structural Health Monitoring*, 2015;14(5):532-543.
2. Liu Z., Sun K., Song G., He C., Wu B. Damage localization in aluminum plate with compact rectangular phased piezoelectric transducer array. *Mechanical Systems and Signal Processing*, 2016;70-71:625-636.
3. Hall J., Michaels J. Multipath ultrasonic guided wave imaging in complex structures. *Structural Health Monitoring*, 2015;14(4):345-358.
4. Zima B., Rucka M. Application of wavelet transform in analysis of guided wave propagation signals for damage detection in a steel plate. *Diagnostyka*, 2015;16(2):43-48.
5. Kędra R., Rucka M. Diagnostics of bolted lap joint using guided wave propagation. *Diagnostyka*, 2014;15(4):35-40.
6. Mazzotti M., Bartoli I., Marzani A. A coupled SAFE-2.5D BEM approach for the dispersion analysis of damped leaky guided waves in embedded waveguides of arbitrary cross-section. *Utrasonics*, 2013;53(7): 1227-1241.
7. Li D., Zhang S., Yang W., Zhang W. Corrosion monitoring and evaluation of reinforced concrete structures utilizing the ultrasonic guided wave technique. *International Journal of Distributed Sensor Networks*, 2014;2014:1-9.
8. Zou S., Cheng J., Yue R., Sun. Grout quality and its impact on guided ultrasonic waves in grouted rock bolts. *Journal of Applied Geophysics*, 2010;72:102-106.
9. Aggelis D.G., Kleitsa D., Iwamoto K., Shiotani T. Elastic wave simulation in ground anchors for the estimation of pre-stress. *Tunnelling and Underground Space Technology*, 2012;30:55-63.
10. Pavlakovic B.N., Lowe M.J.S., Cawley P. High-frequency low-loss ultrasonic modes in imbedded bars. *Journal of Applied Mechanics*, 2001;68:67-75.
11. Wang C., He W., Ning J., Zhang C. Propagation properties of guided wave in the anchorage structure of rock bolts. *Journal of Applied Geophysics*, 2009;69:131-139.
12. Rucka M., Zima B. Elastic wave propagation for condition assessment of steel bar embedded in mortar, *International Journal of Applied Mechanics and Engineering*, 2015;20(1):159-170.
13. Zima B., Rucka M. Wave propagation in damage assessment of ground anchors. *Journal of Physics: Conference Series*, 2015;628: article number: 012026 (8 pages).
14. Pochhammer L. Beitrag zur Theorie der Biegung des Kreiscylinders. *Journal fur die reine und angewandte Mathematik*, 1878;81:33-61.
15. Chree C. The equations of an isotropic elastic solid in polar and cylindrical coordinates, their solutions and applications. *Transactions of the Cambridge Philosophical Society*, 1889;14:250-369.
16. Lai J-L., Dowell E.H., Tauchert T.R. Propagation of harmonic waves in composite elastic cylinder. *The Journal of the Acoustical Society of America*, 1971;49(1):220-228.
17. McNiven H.D., Sackman J. L., Shah A.H. Dispersion of Axially Symmetric waves in composite, elastic rods. *The Journal of the Acoustical Society of America*, 1963;35(10):1602-1609.
18. Seco F., Jimenez A.R. Modelling the Generation and Propagation of Ultrasonic Signals in Cylindrical Waveguides. *Ultrasonic Waves*, Dr Santos (Ed.), ISBN: 978-953-51-0201-4, 2012, 1-28.

Received 2016-04-05
Accepted 2016-06-12
Available online 2016-09-19

Beata ZIMA, M.Sc. graduated civil engineering at the Faculty of Civil and Environmental Engineering of Gdansk University of Technology. Since October 2014 she continues her education as a Ph.D. student. She mainly deals with damage detection using wave propagation.

Magdalena RUCKA, Ph.D., D.Sc. is an assistant professor at the Department of Mechanics of Materials of Gdansk University of Technology. Her scientific interests are focused on dynamic of structures, wave propagation and development of new techniques for damage detection and structural health monitoring.